Cav03-GS-9-005

Fifth International Symposium on Cavitation (CAV2003)
Osaka, Japan, November 1-4, 2003

THREE-DIMENSIONAL UNSTEADY CAVITATION EFFECTS ON A SINGLE HYDROFOIL AND IN A RADIAL PUMP – MEASUREMENTS AND NUMERICAL SIMULATIONS

PART TWO: NUMERICAL SIMULATION

M. Frobenius, R. Schilling
Institute of Fluidmechanics
Munich University of Technology
frobenius@lhm.mw.tum.de

R. Bachert, B. Stoffel, G. Ludwig
Chair of Turbomachinery and Fluidpower
Darmstadt University of Technology
rbachert@tfa.tu-darmstadt.de

ABSTRACT

For the numerical simulation of cavitating flows a cavitation model was implemented in the CFD-Code NS3D developed at the Institute of Fluid Mechanics, Munich University of Technology.

The 2D flow around a hydrofoil with a circular leading edge and the 3D flow around a hydrofoil with swept leading edge are simulated. The results are compared with experimental data, see part one. The unsteady cavitating flow is characterized by the frequent shedding of vapor clouds caused by the development of a re-entrant jet. The shape of the cavitation zone, the frequency of the bubble cloud shedding and the pressure distributions on the surface of the hydrofoil agree well with the experimental findings. For industrial applications also a steady cavitation model has been developed by modifying the void fraction transport equation of the original model. Steady state simulations with the modified model are performed for the cavitating flow through a centrifugal pump impeller of low specific speed. Simulated head-drop-curves are compared with the measured ones and show a good agreement. The $NPSH_{3\%}$-values for a head-drop of three percent coincide well with the experimental results.

INTRODUCTION

In the design and use of hydraulic turbomachines cavitation and the effects related to cavitation are playing an important role. Of special interest are the mechanisms of cavitation yielding to noise generation, loss of efficiency and erosive damage of the exposed surfaces. To avoid or to reduce the effects of cavitation by design and operation, there is a persistent need of improving the detailed understanding of the physical phenomena and their modelization for numerical calculations.

For this, a cavitation model has been integrated in the CFD-Code NS3D developed at the Institute of Fluidmechanics, Munich University of Technology. The CFD-Code solves the Reynolds-averaged Navier-Stokes equations coupled with a single fluid model for the cavitation. For modeling the cavitation the bubble dynamic approach developed by SAUER [1] is applied, which is based on a modified Volume of Fluid (VoF)-Method and considers the cavitating structures as a homogeneous liquid-vapor mixture, with a no-slip condition between the two phases.

The application of the developed code to simulate the cavitating flow around a single hydrofoil and through a centrifugal pump impeller is presented. The unsteady behaviour of the cavitation occuring at the suction side of the hydrofoil is studied and the capability of the cavitation model to simulate the mechanism of self-oscillation is shown. Also steady state simulations of the cavitating flow around the hydrofoil and through the pump impeller are performed. The predicted head-drop curves are compared with the measured ones.

In part I of our common paper, the experimental configurations, methods and results are presented. Part II presents the self developed CFD-code, the modelization of cavitating flows and numerical results in comparison with experimental results gained for the hydrofoil and the test pump.

NOMENCLATURE

Symbols:

f	[1/s]	frequency
H	[m]	head
	$H = \frac{p_{s1} - p_{s2}}{\rho g}$	
k	[m^2/s^2]	turbulent kinetic energy
l	[m]	length
n	[$^1/_{min}$]	speed of rotation
n_{cell}	[-]	number of bubbles per computing cell
n_0	[-]	number of bubbles per m^3 fluid
$NPSH$	[m]	Net Positive Suction Head
	$NPSH = \frac{p_0 - p_D}{\rho g} + \frac{u_{in}^2}{2g}$	
$NPSH_{3\%}$	[m]	Three percent head drop
$NPSH_{IC}$	[m]	incipient head drop
p	[bar]	static pressure
p_B	[bar]	static pressure at the bubble boundary

p_0	[bar]	static pressure at the suction nozzle
p_{s1}, p_{s2},	[bar]	static pressure at the inlet, outlet
p_∞	[bar]	static pressure at the ambient cell
p_v	[bar]	vapor pressure
q	[-]	relative flow rate
$q = Q/Q_{opt}$		
Q	[m³/h]	flow rate
R	[m]	bubble radius
Re	[-]	Reynolds number
$\mathrm{Re} = \frac{u_{in}\, l_{chord}}{\nu}$		
Str	[-]	Strouhal-number
$Str = \frac{f_c l_c}{u_c}$		
T	[K]	temperature
Tu	[-]	turbulent intensity
t	[s]	time
u	[m/s]	velocity
u_{in}	[m/s]	inflow velocity
u_c	[m/s]	mean liquid velocity at the interface of the cavitation zone
V_v ,V_{fl}	[m²]	cell volume occupied by vapor, fluid
V_{cell}	[m²]	total cell volume
x	[m]	space coordinate
α		vapor void fraction
β	[°]	leading edge sweep angle of hydrofoil
δ		delta function
ε	[m²/s³]	dissipation rate
η	[-]	efficiency
μ	[kg/ms]	molecular viscosity
μ_t	[kg/ms]	turbulent viscosity
ν	[m²/s]	kinematic viscosity
ρ	[kg/m³]	density
σ_0	[N/m]	surface tension
σ	[-]	cavitation number
$\sigma = \frac{p_\infty - p_v}{\frac{1}{2}\rho u_{in}^2}$		
τ	[kg/ms²]	viscious stress tensor

Subscripts:

cor	corrected
i,j	coordinate index
l	liquid
Opt	at design point of pump
v	vapor
∞	reference value (at inlet of test section)
in	inflow

CAVITATION MODELING

The cavitation model, originally developed by SAUER [1], is based on bubble dynamics and describes the complicated bubble growth and collapse. The bubbles originate from very small nuclei, particles or air bubbles, which are existing in the fluid flow. When the nuclei reach the low pressure region, i.e. the suction peak, they grow to vapor bubbles while they are convected downstream. The bubbles collapse, when they reach the region of higher pressure.

The model resolves the dispersed structure of the bubble cloud and calculates the production, i.e. the bubble growth, the destruction, i.e. the bubble collapse, and the convection of the vapor phase.

The vapor-liquid flow described by a single-fluid model is treated as a homogeneous bubble-liquid mixture, so only one set of equations is needed to simulate cavitating flows:

$$\frac{\partial}{\partial t}(\rho) + \frac{\partial}{\partial x_i}(\rho \vec{u}_i) = 0\,, \tag{1}$$

$$\frac{\partial}{\partial t}(\rho \vec{u}_i) + \frac{\partial}{\partial x_i}(\rho \vec{u}_j \vec{u}_i) = -\frac{\partial}{\partial x_i}(p) + \frac{\partial \tau_{ij}}{\partial x_i}\,. \tag{2}$$

The constitutive relations for the density and dynamic viscosity of the mixture are:

$$\begin{aligned} \rho &= \alpha \cdot \rho_v + (1-\alpha)\cdot \rho_l\,, \\ \mu &= \alpha \cdot \mu_v + (1-\alpha)\cdot \mu_l\,. \end{aligned} \tag{3}$$

The subscripts l and v stand for the properties of pure liquid and pure vapor, which are supposed to be constant.

Additionally, a transport equation for the vapor fraction α is required. The vapor void fraction α can be written as

$$\alpha = \frac{V_v}{V_{cell}} = \frac{n_{cell} \cdot \frac{4}{3}\pi R^3}{V_v + V_l} = \frac{n_0 \cdot \frac{4}{3}\pi R^3}{1 + n_0 \cdot \frac{4}{3}\pi R^3}\,, \tag{4}$$

where V_{cell} is the volume of the computational cell, V_v and V_l are the volumes occupied by vapor and liquid, n_{cell} is the number of bubbles in the computational cell, whereas n_0 is the number of bubbles or nuclei per cubic meter. That means n_0 is a constant parameter depending on the considered liquid.

Considering spherical bubbles and neglecting the bubble-bubble interaction and coalescence, the Rayleigh-Plesset equation can be used to model the process of bubble growth and collapse:

$$R\frac{d^2R}{dt^2} + \frac{3}{2}\left(\frac{dR}{dt}\right)^2 = \frac{p_B(T) - p_\infty}{\rho_l} - \frac{2\sigma_0(T)}{\rho_l R} - 4\frac{\mu_l}{\rho_l R}\frac{dR}{dt}\,. \tag{5}$$

As the pressure difference $p_B(T)$-p_∞ is assumed to be large and the viscosity, the surface tension and inertia effects are neglected, the Rayleigh-equation is used to describe the so-called inertia controlled bubble growth:

$$\left(\frac{dR}{dt}\right)^2 = \frac{2}{3}\frac{p_B(T) - p_\infty}{\rho_l}\,. \tag{6}$$

In equation (6) $p_B(T)$ is the pressure in the liquid at the bubble boundary which is assumed equal to the vapor pressure p_v, which depends on the temperature. p_∞ is the ambient cell pressure.

The total derivative of the void fraction results in

$$\frac{d\alpha}{dt} = (1-\alpha)\frac{4\pi n_0 R^2}{1 + n_0 \frac{4}{3}\pi R^3}\frac{dR}{dt}\,. \tag{7}$$

The transport equation for the void fraction is extended by a source term on the right hand side:

$$\frac{\partial \alpha}{\partial t} + \frac{\partial(\alpha u_i)}{\partial x_j} = \frac{d\alpha}{dt} + \alpha\frac{\partial}{\partial x_i}(\vec{u}_i)\,. \tag{8}$$

Because of the bubble growth, the velocity field is no longer divergence-free, the continuity equation is used in its non-conservative form:

$$\frac{\partial}{\partial x_i}(\vec{u}_i) = -\frac{1}{\rho}\left(\frac{\partial \rho}{\partial t} + \vec{u}_i \frac{\partial \rho}{\partial x_i}\right) = -\frac{1}{\rho}\frac{d\rho}{dt} \approx \frac{\rho_l - \rho_v}{\rho}\frac{d\alpha}{dt}. \qquad (9)$$

With this expression and equation 7 the transport equation for the void fraction can be written as

$$\frac{\partial \alpha}{\partial t} + \frac{\partial(\alpha u_i)}{\partial x_j} = \frac{n_0}{1 + n_0 \frac{4}{3}\pi R^3} \cdot \frac{d}{dt}\left(\frac{4}{3}\pi R^3\right). \qquad (10)$$

The source terms for the vapor fraction equation and for the pressure correction equation have the same form. The continuity equation can be used in its incompressible form, only an additional source term has to be considered. A more detailed description of the implementation of the cavitation model can be found in [2].

NUMERICAL MODEL

The cavitation model was implemented in the CFD-Code NS3D developed at the Institute of Fluidmechanics, Munich University of Technology. The code is based on a co-located, cell-centred and block-structured finite volume method using the SIMPLE algorithm. For the interpolation of the mass fluxes at the cell faces, RHIE & CHOW's method is used [3]. The discretization of the convective terms is realized by the second order MINMOD-scheme of HARTEN [2]. The code is able to calculate general multiblock topologies with matching and non-matching interfaces in 2D and 3D domains. The parallelization of the code is realized by means of MPI-libraries (Message Passing Interface), and the sets of linear equations are solved using the Strongly Implicit Procedure of STONE [5]. For the simulation of cavitating flows a standard k-ε-model [6] assuming a density variable, but incompressible flow field and a nonlinear eddy-vicosity model suggested by LIEN et al. [7] are used. Both models use wall functions. For unsteady simulations a three-level implicit time-discretization-scheme is used, so the time step is not limited. A detailed description of the code can be found in SKODA [8].

The flow is assumed isothermal and fluid properties are supposed to be constant at a given temperature for the entire flow domain. For all simulations presented, cold water at a constant temperature $T = 296\ K$ with 10^8 nuclei per m^3 water having a minimal nuclei radius of *30* microns is assumed to match the experimental conditions. The vapor density was set to a constant value of $\rho_v = 0.1\ kg/m^3$ and the vapor pressure to $p_v = 2809\ Pa$ corresponding to the water temperature $T = 296\ K$. The incoming fluid has a turbulence intensity of $Tu = 2\%$. At the inlet of the computational domain the flow rate is prescribed, at the outlet a "Dirichlet"-condition for the static pressure is assumed.

RESULTS FOR THE SINGLE HYDROFOIL

For the simulation of the cavitating flow around the hydrofoil described in part I of our common paper a 4-block-structured grid was used, see Figure 1. The inner O-grid around the hydrofoil is connected to its neighbour-block by a non-matching block-interface, which allows a finer resolution of the inner block without changing the size of the other blocks. For the O-Grid three different resolutions have been used, see Table 1.

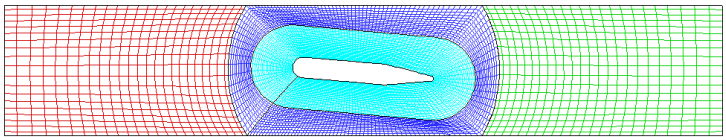

Figure 1: Multiblock grid topology for the simulation of the CLE-hydrofoil

Grid size	Number of cells
Coarse	157 x 30
Mean	197 x 45
Fine	237 x 60

Table 1: Different grid resolutions for the O-grid

For the three grid resolutions the nondimensional wall distance y^+ was set to values between *30* and *300*, so that the logarithmic wall law can be applied. The y^+-values for the three grids are ploted in Figure 2.

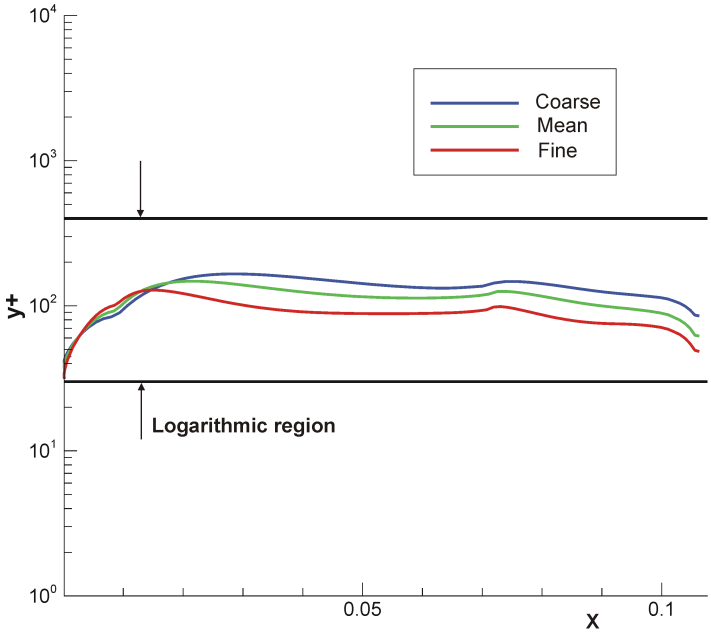

Figure 2: Dimensionless wall distance y^+ for different grid resolution

A constant inflow velocity of $u_{in} = 13\ m/s$ corresponding to a Reynolds-number of $Re = 1.3 \cdot 10^6$ was assumed at a cavitation number of $\sigma = 2.0$. An example of the simulated unsteady behaviour of the 2D cavitating flow around the hydrofoil with an angle of attack of *5°* is shown in Figure 3. Here successive shapes of the cavitation zone obtained during a complete cavitation cycle are shown. The flow is from left to right. The plotted velocity vectors show the development of the re-entrant-jet and the shedding of the cavitation cloud. The self-oscillating

behaviour shows a characteristic frequency of *125 Hz*, which corresponds to a Strouhal number of $Str = f_c \cdot l_c / u_c \cong 0.2$. This is in good agreement with the experimental observation of HOFMAN [9], who found at the same profile Strouhal-numbers in the range of $Str = 0.2 \ldots 0.25$, depending on the flow velocity.

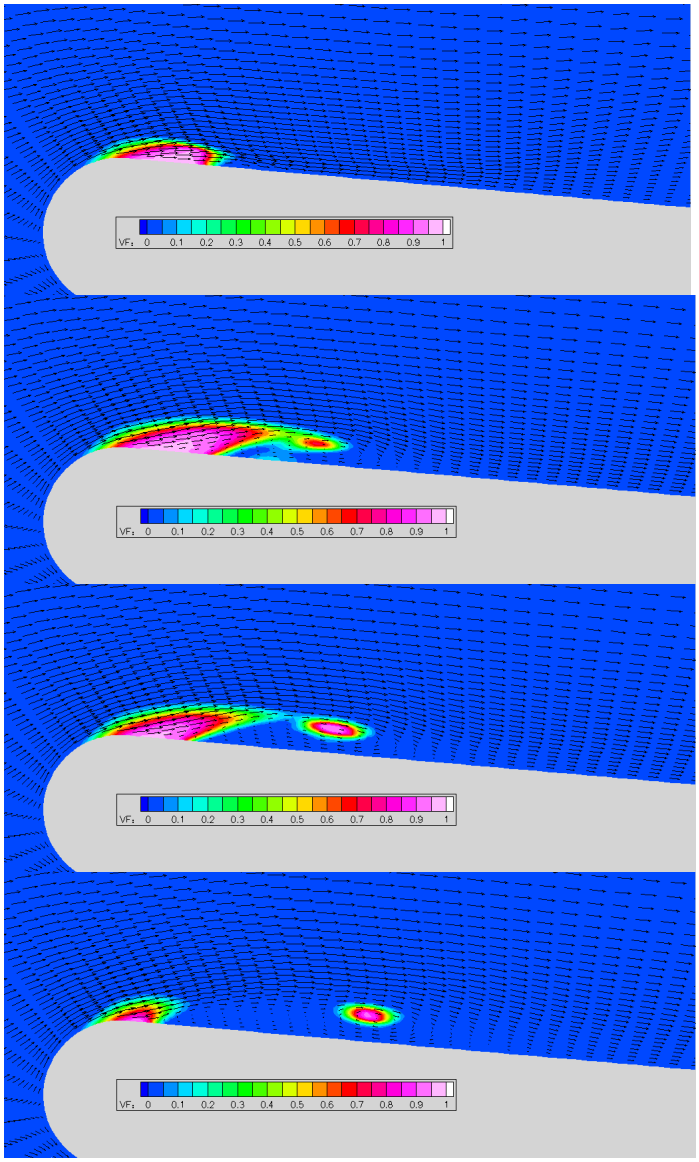

Figure 3: Predicted vapor void fraction and velocity vectors during one period if the unsteady cavitation loop. CLE-foil with $Re = 1.3 \cdot 10^6$, σ=2.0

The computed shedding frequency depends on the grid resolution and on the chosen time-step. Figure 4 shows the time-step-dependency of the computed Strouhal number for different grids for an inflow veocity of u_{in}=13 m/s. For smaller time-steps the Strouhal number approaches a constant value near the experimental value. With higher grid resolutions the predicted Strouhal number is nearer to the experimental one. For higher time-steps the computed cavitating flow becomes steady.

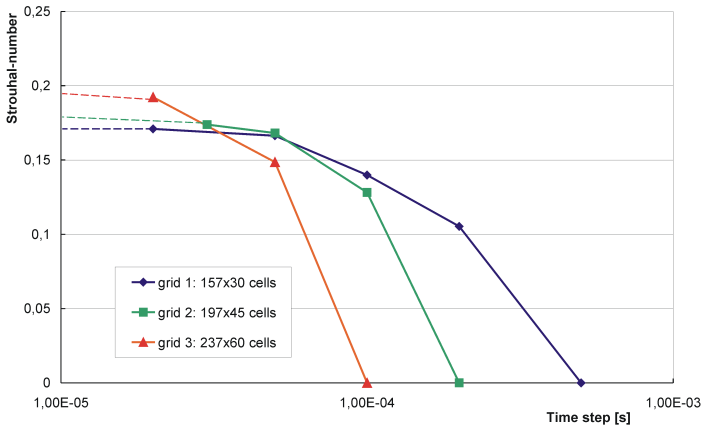

Figure 4: Influence of the time-step and the grid resolution on the Strouhal-number of the cavitation cycle

Unsteady simulations of the cavitating flow are very time-consuming, so for industrial use steady-state-simulations are preferred. For steady-state simulations the source term in the vapor phase fraction transport equation is modified to account for the different time-scales of the bubble growth and collapse:

$$\frac{\partial \alpha}{\partial t} + \frac{\partial (\alpha u_i)}{\partial x_j} = C_{cor} \frac{n_0}{1 + n_0 \frac{4}{3}\pi R^3} \cdot \frac{d}{dt}\left(\tfrac{4}{3}\pi R^3\right), \qquad (11)$$

$$\text{with} \quad C_{cor} = \begin{cases} 50 & \text{for bubble growth} \\ 1/50 & \text{for bubble collapse} \end{cases}$$

Steady simulations were performed for the cavitating flow around the 3D-wings with swept leading edge. Figure 5 compares the predicted cavitation zone with the mean value of the experimentally observed brightness of the cavitation zone. Both the simulation and the experiment show a shorter cavitation zone at the left side of the profile, looking in flow direction. At the right side the cavitation zone grows and separates. During the experiments cavitation cloud shedding is observed.

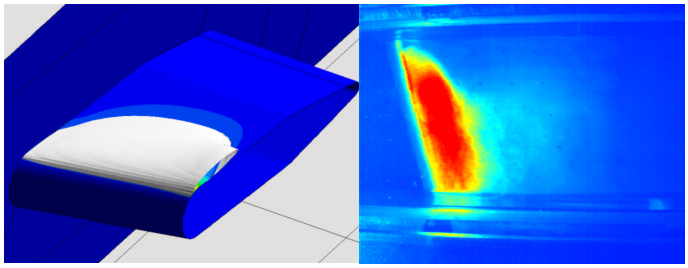

Figure 5: Comparison of the predicted (left) and experimentally observed (right) extension of the cavitation zone on the CLE-hydrofoil with an angle of attack of 5° and a sweep angle β=15° for σ= 2.5 and $Re = 1.3 \cdot 10^6$

This effect is clearly visible when comparing the velocity vector plots of the PIV/LIF-meassurement in part I of the paper with the predicted vector plot, see Figure 6. The plots are taken

at a position *5 mm* off the front plate. In the experiments as well as in the simulation a re-entrant-jet is occuring. This is not the case on the left side of the profile, where the cavitation region remains attached to the hydrofoil. Thus the steady-state simulation allows a detection of this kind of cavitation.

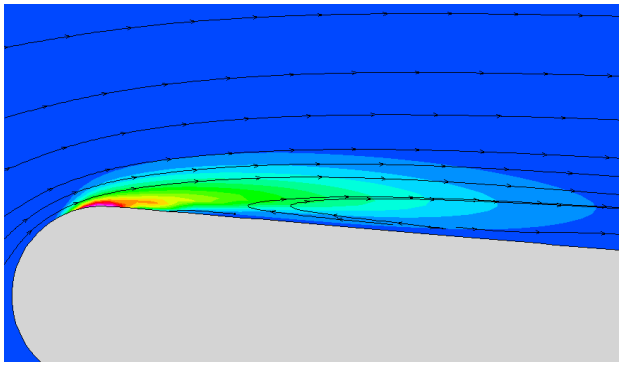

Figure 6: Contour-plot of the predicted vapor void fraction and computed streamlines near the front plate of the CLE-hydrofoil for $\sigma = 2.0$

In case of the hydrofoil with the sweep angle of $\beta=25°$, the 3D-effect becomes even stronger due to the higher cross component of the velocity. Figure 7 compares the extension of the cavitation zone predicted by the CFD-code with CCD-images at the same flow conditions.

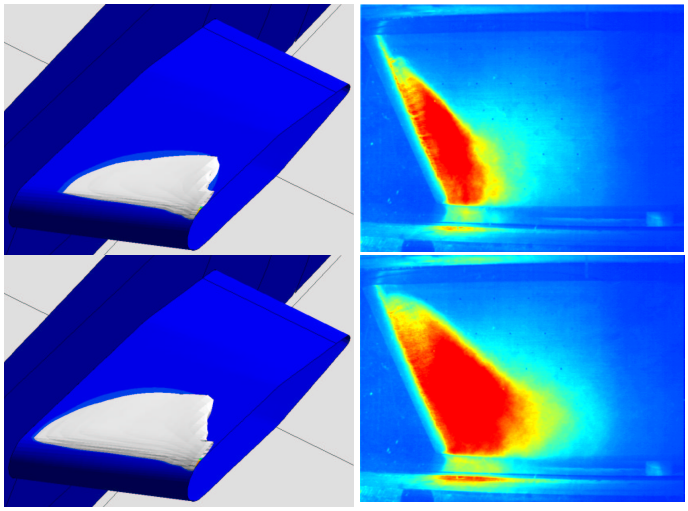

Figure 7: Comparison of the predicted (left) and experimentally observed (right) extension of the cavitation zone on the CLE-hydrofoil with an angle of attack of *5°* and a sweep angle $\beta=25°$ for $\sigma = 2.5$ (top) and $\sigma = 2.0$ (bottom)

A comparison of the calculated and measured averaged re-entant-jet velocity is given in Table 2. Generally, the re-entrant jet velocities predicted by the steady-state simulation are smaller than the measured ones, especially for the sweep angle of $\beta=15°$. The 3D-character of the flow is more distinct with the $\beta=25°$ sweep angle.

$u_{re\text{-}entant}$ [m/s]	β=15°		β=25°	
	EXP	SIM	EXP	SIM
σ=2.5	-3.3	-0.6	-2.2	-1.9
σ=2.3	-4.2	-1.3	-4.6	-3.3
σ=2.0	-3.3	-1.7	-3.3	-2.5

Table 2: Comparison of the predicted and measured averaged re-entrant-jet velocities near the front plate

RESULTS FOR THE RADIAL IMPELLER

The geometry of the radial pump impeller is described in part I of the common paper. For the simulation of the cavitating flow through the radial impeller a free impeller calculation was performed, which means, that only one flow channel delivering into the vainless radial diffuser is considered. The shape of the meridional contour, the meridian plot and the conformal mapping of the 3D grid with *112,000* cells used for the simulation is shown in Figure 8. The dimensionless wall distance y^+ was set to values between *30* and *300*, so that the logarithmic wall law could be applied.

For the simulation of the cavitating flow, first a stationary calculation at a high pressure level is performed to ensure non-cavitating conditions in the whole computational domain. Then, the outflow pressure is lowered in small steps. During this process, vapor structures appear and grow in the regions of low static pressure. The more the pressure level is lowered, the more the cavitation zone grows, influencing the impeller head.

Simulations are performed for a rotational speed of $n=1750$ $^1/_{\min}$ and, the design flow rate beeing $Q=126\ m^3/h$. The flow rate is set by the inflow boundary condition, the static pressure is defined at the outlet boundary.

To compare the predicted and measured head drop curves, the impeller head H defined by

$$H = \frac{p_{s2} - p_{s1}}{\rho \cdot g}, \qquad (12)$$

which is plotted against the net positive suction head NPSH

$$NPSH = \frac{p_0 - p_{sat}}{\rho \cdot g}. \qquad (13)$$

The head H computed from the CFD simulation results by averaging the static pressure at the inlet p_{s1} and the outlet p_{s2} of the computational domain and employing equation 11.

The NPSH-value is defined as the total pressure p_0 of the fluid at the suction nozzle above the vapor pressure p_v of the fluid depending on the fluid temperature *T*.

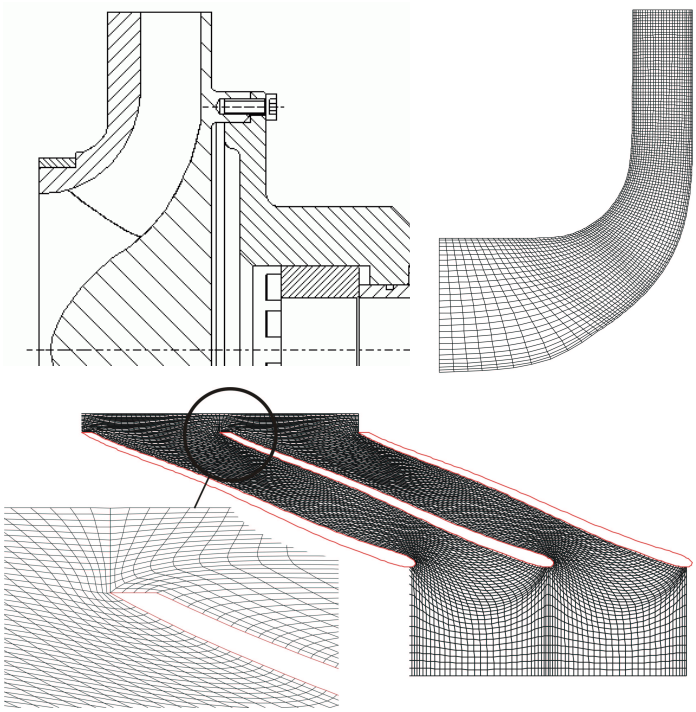

Figure 8: Meridional section of the radial impeller (top left); Meridional section of the computational grid (top right); conformal mapping of the computational grid

The computed relative head drop curve for a speed of $n=1750\ ^{1}/_{min}$ considering the design point Q_{opt} is shown in Figure 9. In general, the deviation between the predicted and the measured head drop curve is small. The predicted head drop occurs almost at the same NPSH-value as the measured one.

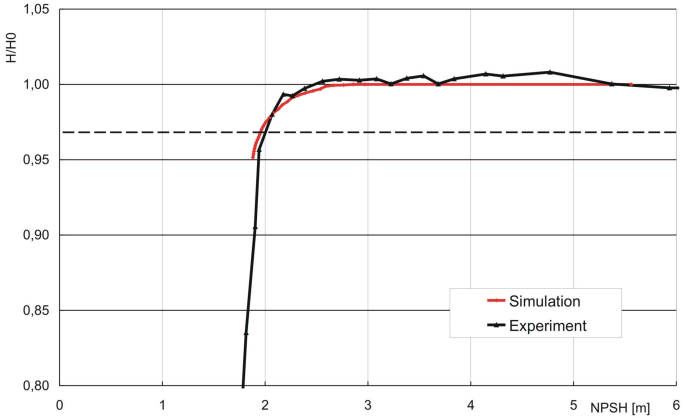

Figure 9: Predicted and measured head drop curves for *n=1750 1/min* and $Q=Q_{opt}$

Figure 10 shows the comparison of the predicted and measured $NPSH_{3\%}$ depending on the relative flow rate and the computed $NPSH_{IC}$-values for $n=1750\ ^{1}/_{min}$. The predicted values for incipient cavitation and for the three percent head drop correlate well with the experiments.

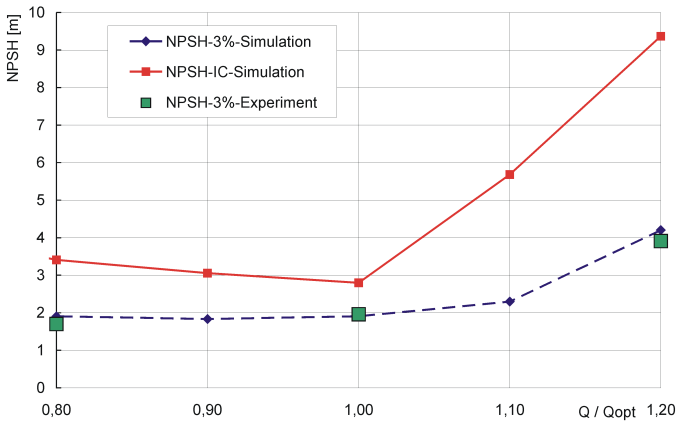

Figure 10: Predicted and measured $NPSH_{3\%}$-curves and computed $NPSH_{IC}$-values for *n=1750 1/min*

For a comparison with the experimental results measured for $n=2000\ ^{1}/_{min}$ the computed results are scaled up. In Table 3 the computed $NPSH_{IC}$-value for $n=1750\ ^{1}/_{min}$ and the scaled-up value for $n=2000\ ^{1}/_{min}$ are compared with the experimental values

$NPSH_{3\%}$ [m]	EXP	SIM
n=1750 $^{1}/_{min}$	2,02	1,96 simulated
n=2000 $^{1}/_{min}$	2.60	2. 56 scaled up

Table 3: Comparison of the measured and predicted $NPSH_{3\%}$-values for $n=1750\ ^{1}/_{min}$ and $n=2000\ ^{1}/_{min}$

CONCLUSIONS

A bubble dynamic cavitation model has been integrated in the NS3D-Code. Unsteady and steady simulations have been performed for 2D and 3D cavitating flows around hydrofoils. Based on these experiencies the cavitating flow through a centrifugal pump impeller has been simulated in a good agreement with the measurements.

The results of the unsteady simulation show the typical development of a re-entrant jet and the bubble cloud shedding. The predicted shedding frequencies agree well with the experiments performed by the team of Prof. Stoffel. The swept 3D hydrofoil shows sheet cavitation on one side of the profile and cloud cavitation on the other. The size of the cavitation area and the separation of the cavitation cloud are clearly predicted by the CFD-code. The computed head-drop curves and $NPSH_{3\%}$-values show a very good agreement with the experiments.

ACKNOWLEDGMENTS

We would like to thank the Forschungsfond Pumpen (Pump Research Foundation) of VDMA (Federation of the German Engineering Industries) for financing and supporting the project. Special thanks from the numerics group of the Institute of Fluid Mechanics, Munich University of Technology to their colleagues of the Chair of Turbomachinery and Fluidpower at Darmstadt

University of Technology, for the efficient collaboration during the whole project duration.

REFERENCES

[1] SAUER, J.: *Instationär kavitierende Strömungen – Ein neues Modell basierend auf Front Capturing (VOF) und Blasendynamik*, Dissertation, Universität Karlsruhe, 2000

[2] FROBENIUS, M.; SCHILLING, R.; FRIEDRICHS, J. KOSYNA: *Numerical and experimental investigations of the cavitating flow in a centrifugal pump impeller*, Proceedings of the ASME FEDSM, Montreal, 2002

[3] RHIE, C.M.; CHOW, W.L.: *A numerical study of the turbulent flow past an isolated airfoil with trailing edge separation*. AIAA Journal 21 (1983), pp 1525-1532.

[4] HARTEN, A.: *High resolution schemes for hyperbolic conservation laws*. Journal of Computational Physics 49, pp. 357 – 393, 1983

[5] STONE, H.L.: *Iterative solution of implicit approximations of multidimensional partial differential equations*, S.I.A.M. Journal of Scientific and Statistical Computing 5, no.3 pp. 530-558, 1968

[6] LAUNDER, B.E.; SPALDING, D.B.: *Mathematical Models of Turbulence*, Academic Press, London, 1972.

[7] LIEN, F.S.; CHEN, W.L.; LESCHZINEER, M.A.: *Low-Reynolds-number eddy viscosity modeling based on non-linear stress-strain / vorticity relations.*, Proceedings of the 3rd Int. Symposium on Engineering Turbulence Modeling and Experiments, Kreta, 1996

[8] SKODA, R.: *Numerische Simulation abgelöster und transitionaler Strömungen in Turbomaschinen*, Dissertation, TU München, 2003

[9] HOFMANN, M.: *Ein Beitrag zur Verminderung des Potentials kavitierender Strömungen*, Dissertation, TU Darmstadt, 2001